



Inhibition of Corrosion-Related Reduction Processes via Chromium Monolayer Formation

William J. Clark and Richard L. McCreery*^z

Department of Chemistry, The Ohio State University, Columbus, Ohio 43210-1185, USA

The oxygen reduction reaction (ORR) was examined on copper, platinum, and glassy carbon electrodes, with regard to its inhibition by exposure of the electrode to chromate ion (Cr^{VI}) in NaCl solution. All three electrode materials exhibited a mass transport limited current for the ORR at sufficiently negative potentials, but this current was strongly inhibited in the presence of Cr^{VI} . Inhibition persisted in Cr^{VI} -free solution after the electrode was rinsed thoroughly, indicating that Cr^{VI} formed an irreversibly adsorbed inhibiting layer. A reduction peak observed in Cr^{VI} solution had an area of 1.1–2.5 mC/cm^2 , and the area varied little with Cr^{VI} concentration, electrode material, and potential in the range of +0.2 to –0.6 V vs. Ag/AgCl . This reduction peak is attributed to Cr^{III} formation, and corresponds to formation of approximately a monolayer of Cr^{III} oxyhydroxide. Once formed, this Cr^{III} monolayer inhibits both O_2 reduction and further reduction of Cr^{VI} . The onset of monolayer formation at about +0.25 V vs. Ag/AgCl is the same as the potential of the onset of ORR inhibition in dilute Cr^{VI} . The monolayer also decreases the electron transfer rate to ferrocene and $\text{Ru}(\text{NH}_3)_6^{+3}$, which are known to be outer sphere redox systems that do not require adsorption to the electrode surface. The results indicate that the adsorbed Cr^{III} film formed by Cr^{VI} reduction is a powerful inhibitor of oxygen reduction, due both to occupation of active chemisorption sites and to inhibition of electron transfer. In the context of corrosion protection, Cr^{VI} acts as a “site-directed” irreversible inhibitor which migrates to active sites for the ORR, then is reduced to Cr^{III} , and forms a permanent inhibiting monolayer.

© 2002 The Electrochemical Society. [DOI: 10.1149/1.1494825] All rights reserved.

Manuscript submitted October 10, 2001; revised manuscript received February 27, 2002. Available electronically July 12, 2002.

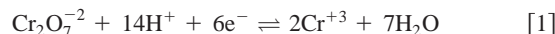
Continuing efforts to reduce exposure to materials containing hexavalent chromium have necessitated the drive to eliminate chromium as a corrosion inhibitor for aluminum alloys. Better understanding of the inhibition mechanism of chromium potentially will enable better design of replacements. The investigations of chromium oxyanion protection of aluminum alloys have been dominated by studies of the inhibition of the dissolution half-reaction (anodic inhibition) of the corrosion process. More recently, the issues of cathodic inhibition such as the role of chromium in the inhibition of the reduction of oxygen have started to be investigated.^{1–3} The kinetics of the oxygen reduction reaction (ORR) on copper-bearing intermetallic compounds present in aluminum alloy AA2024-T3 have been examined in the presence of a chromate conversion coating.¹ The oxygen reduction reaction rate was reduced for conversion coated electrodes made of these intermetallics, although the role of the conversion coating was unclear. Inhibition of cathodic reactions on Cu-containing aluminides was attributed to hexavalent chromium adsorption in another recent study.² Further, separation of anodic and cathodic portions of the corrosion process was achieved by the use of a split-cell with various combinations of aluminum, copper, and aluminum alloy (AA2024-T3) electrodes.³ Dilute solutions of chromate strongly inhibited the ORR on copper and AA2024-T3 surfaces, and inhibition persisted after Cr^{VI} was removed from the solution.

The reduction of Cr^{VI} to Cr^{III} has been shown to be an integral part of the formation process of chromium conversion coatings (CCC). Previous studies have revealed the mechanism for CCC formation and its composition, as well as its distribution on matrix and intermetallic particles.^{4–7} The storage and release of Cr^{VI} in CCC films has been invoked to explain the self-healing properties of chromate coatings, whereby active inhibitor is released by the CCC in response to a scratch or defect.^{8,9} Cr^{VI} migration to exposed alloy provides remote protection of newly formed coating defects, possibly years after initial coating application. Although past studies of CCC formation and behavior explain some of the important features of chromate containing films for corrosion protection, they did not directly investigate the corrosion inhibition mechanism.

While the copper containing intermetallic phases have been im-

plicated in both cathodic and anodic corrosion reactions,¹⁰ the present work addresses cathodic inhibition of the ORR. In particular, how does exposure to Cr^{VI} inhibit the ORR on Cu, Cu-containing intermetallic phases, and redistributed Cu particles on AA2024-T3? We noted previously that ORR inhibition in a split cell was preceded by a cathodic current spike tentatively attributed to the reduction of Cr^{VI} to Cr^{III} .³ Is this cathodic current spike involved in ORR inhibition?

Chromate reduction has been studied in the context of electroplating and industrial chlorate production, and the reactions are complex.¹¹ Although the overall stoichiometry is well known (Reaction 1), the multiple H^+ and e^- transfers require a very complex sequence of fundamental reactions



Previous studies of the Cr^{VI} reduction mechanism were conducted under conditions similar to industrial processes (acidic or strongly basic), rather than the near neutral or acidic chloride solutions relevant to corrosion. However, several observations relevant to the present study are available. Kolthoff *et al.* first reported the formation of a “unimolecular film of Cr^{III} on the [rotating platinum] electrode.”¹¹ This film inhibited numerous redox systems (under varying solution conditions) and was self-inhibiting under mildly acidic conditions (0.001 M HCl). Under strongly acidic conditions (1 M HCl), slight or negligible self-inhibition occurred. Inhibition persisted after rinsing with chromate-free solution. The chlorate process is dependent upon the addition of chromate to prevent the reduction of intermediate hypochlorite ions that are formed. Similar studies on Cr^{VI} reduction have taken place under the highly basic conditions encountered in chlorate production.^{12–16} In 1 M NaOH on platinum and gold electrodes self-inhibition is incomplete, attributed to $\text{Cr}(\text{OH})_4^-$ formation and dissolution, but monolayer films were formed based upon oxidation current measurements. Inhibition of several redox systems was observed ($\text{Fe}[\text{CN}]_6^{3-}$, O_2 , and hypochlorite) in 1 M NaOH.¹²

Reduction of Cr^{VI} in relation to the mechanisms by which chromium oxyanions and conversion coatings provide protection from corrosion has been investigated.¹⁷ Cr^{VI} reduction was examined on platinum electrodes in acidic media (0.18 M H_2SO_4 and 0.022 M H_3PO_4). An insoluble Cr^{III} -phosphate product was formed which inhibited Cr^{VI} reduction after several cycles. It also inhibited the

* Electrochemical Society Active Member.

^z E-mail: mcreery.2@osu.edu

oxidation of ferrocene (in organic solvent), a system that does not require adsorption to the electrode for electron transfer to occur.

The reduction of oxygen, like chromium, is a very complex process and has been studied extensively.¹⁸ The reduction can occur via two or four electrons and has a strong pH dependence. The outer-sphere reduction mechanism (not involving an adsorption step) is kinetically slow, thus catalysis via adsorption to the electrode surface is usually involved. Studies on glassy carbon (GC) electrodes have illustrated one example of how adsorption sites can be blocked and the outer-sphere process observed.¹⁹ For aluminum alloys, oxygen reduction is the primary cathodic reaction that occurs. H^+ reduction can also be an important reaction, but occurs mainly in well-established actively corroding pits having very low local pH.²⁰ An important question to answer regarding the inhibition of oxygen reduction is whether the mechanism involves blockage of adsorption sites or if the electron-transfer process itself is inhibited.

It is not the purpose of the present investigation to provide a detailed mechanism for either Cr^{VI} or O_2 reduction. Rather, we sought to determine the relationship between the reactions of Cr^{VI} and the cathodic inhibition of the ORR under common field conditions encountered by AA2024-T3. The effects of Cr^{VI} on the ORR were examined, initially using Cu electrodes as models of Cu-containing intermetallic compounds and redistributed Cu. In addition, Cr^{VI} reduction was examined on Pt and GC electrodes to permit a wider potential range than possible with Cu.

Experimental

Barnstead NanoPure water with a resistivity of $18 M\Omega \text{ cm}$ was used for rinsing and solution preparation in all cases. NaCl (Fisher Scientific), $K_2Cr_2O_7$ (Alfa Aesar), $Ru(NH_3)_6Cl_3$ (Aldrich), Na_3BO_3 (Fisher Scientific), NaOH (Mallinckrodt), HCl (Fisher Scientific), CH_3CN (Mallinckrodt), and $[CH_3(CH_2)_3]_4BF_4$ (Aldrich) were reagent grade and used as received. Electrodes were commercial Pt or GC (Bioanalytical Systems) or were made from 0.5 mm diam copper wire (99.9% Cu, Aldrich). Copper wire electrodes were attached to standard copper electrical wire with silver epoxy resin (SPI Supplies/Structure Probe Inc.), and embedded in epoxy (Buehler). They were mechanically polished with successively finer Si:C papers (Buehler: 240, 400, 600, 800, 1200 grit), rinsed with water, and dried under a stream of hot air. Prior to each experiment, all electrodes were polished using Al_2O_3 slurries (Buehler, 1.0, 0.3, and 0.05 μm) and rinsed with water.

Hydrodynamic and potentiostatic electrochemical measurements were performed using a Gamry Instruments PC3/300 potentiostat/galvanostat/zero resistance ammeter with Framework (Version 3.11) and DC105 dc corrosion measurement software. Cyclic voltammetry was performed using a Bioanalytical Systems BAS100B electrochemical analyzer using BAS100W software. Experiments were performed using a standard three-electrode electrochemical cell. Experiments in water utilized Ag/AgCl as the reference electrode (potential = 0.197 V vs. normal hydrogen electrode, NHE) and all potentials quoted are with respect to this reference. Experiments in acetonitrile used Ag/Ag⁺ (filling solution: 0.1 M $[CH_3(CH_2)_3]_4BF_4$ in CH_3CN) as the reference electrode. Pt wire was used as the counter electrode. Unless otherwise noted, 0.1 M NaCl served as the background electrolyte for aqueous solutions and 0.1 M $[CH_3(CH_2)_3]_4BF_4$ for acetonitrile. Aerated refers to stirred solutions open to air and deaerated refers to solutions purged with prepurified argon for >15 min. Where noted, solutions were also saturated with extra dry O_2 . Solution additions were made using 0.05 M $K_2Cr_2O_7$ (0.1 M total Cr^{VI}) in 0.1 M NaCl, and 10 mM $Ru(NH_3)_6Cl_3$ as noted in the text and figures. Unless stated otherwise, Cr^{VI} concentrations are stated as total $[Cr^{VI}]$ in the form of $HCrO_4^-$, CrO_4^{2-} , $Cr_2O_7^{2-}$, etc. Unless noted, solutions were unbuffered except by Cr^{VI} itself, resulting in a pH of ~6.

Electrochemical experiments were performed as follows.

Constant potential with Cr^{VI} injection.—The solution was stirred

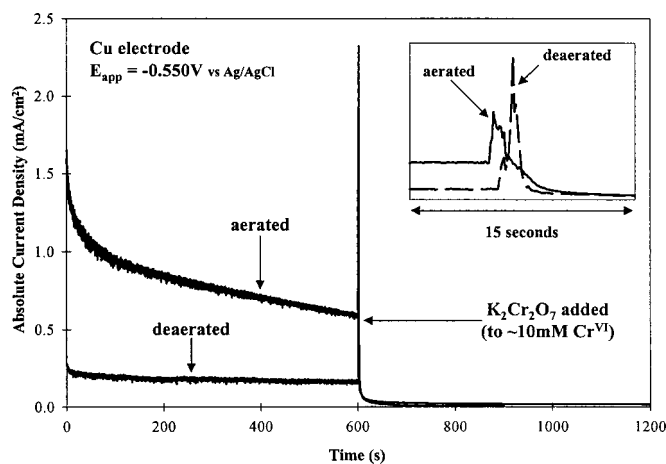


Figure 1. Current response of copper electrode *vs.* time at constant potential (-0.550 V *vs.* Ag/AgCl) in 0.1 M NaCl. The solution was stirred and aerated or deaerated as indicated. Cr^{VI} was injected (to ~ 10 mM) at ~ 600 s. Inset shows response in time frame near Cr^{VI} injection point.

with a magnetic stir bar and aerated or deaerated as noted. The electrode was held at -1.500 V for 60 s to reduce surface oxides before setting to the desired experimental potential. At a specified time an aliquot of analyte was injected into the solution. If the solution was deaerated the injection aliquot was deaerated also. The current response was monitored as a function of time.

Hydrodynamic voltammetry.—The solution was stirred and aerated or deaerated as noted. A magnetic stirrer was used rather than a rotating disk electrode because the variety of electrode materials required a flexible cell and electrode mount. The electrode was held at -1.000 V for 60 s to reduce surface oxides. Potential control was then removed and the electrode allowed to come to its open circuit value for 600 s. Analyte species were added during this step if desired. The potential was then scanned from the open circuit value to -1.300 V at 1 mV/s. Current response was monitored as a function of potential. In some cases, the open circuit potential (OCP) period was omitted and the potential was scanned from $+0.500$ to -1.300 V. Analyte species were added with the potential at positive values if desired.

Potential step.—The solution was stirred and aerated or deaerated as noted. The electrode was held at -1.000 V for 60 s to reduce surface oxides. The potential was then held at $+0.750$ V for a specified time period. Analyte species were added during this step if desired. The potential was then stepped to a specified value and held for a fixed time. The current response was monitored as a function of time. If the electrode was to be used in a subsequent experiment without additional polishing it was removed from the solution under potential control while being rinsed with water.

Cyclic voltammetry.—Experiments were performed in both aqueous and organic media. For aqueous media, the solution was quiescent and oxygenated. The potential was cycled from 0.000 V to either $+1.000$ or -1.000 V in pH 11 buffer (0.1 M BO_3^{3-} / 0.9 M NaCl) at 200 mV/s while observing current response. In some cases, the electrode was pretreated with Cr^{VI} as described in the Results section. For organic media experiments, the solution was quiescent and deaerated. The potential was cycled between -1.000 and $+1.000$ V at 1000 mV/s while observing current response.

Results

Figures 1 and 2 show results of constant/potential hydrodynamic experiments using a copper electrode held at -0.550 V. This potential was chosen due to its proximity to the OCP for AA2024-T3

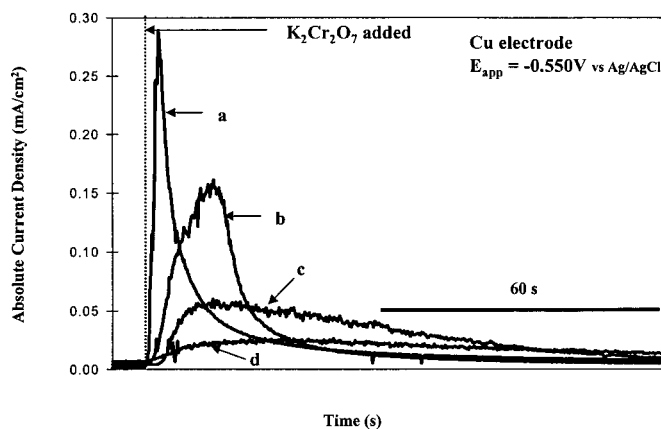


Figure 2. Effect of Cr^{VI} concentration on current response of copper electrode at constant potential (−0.550 V vs. Ag/AgCl) in stirred, deaerated 0.1 M NaCl. At the indicated time Cr^{VI} was injected to (a) 5×10^{-3} M, (b) 5×10^{-4} M, (c) 5×10^{-5} M, and (d) 5×10^{-6} M.

examined in the previous study.³ In Fig. 1 both aerated and deaerated solutions of 0.1 M NaCl are shown. The higher current density before chromate injection for the aerated solution is attributed to the reduction of dissolved oxygen. Upon injection of chromate (to ~10 mM total Cr^{VI}) the current immediately increases and then rapidly decreases for both solutions. The current density of each solution after chromate addition falls to less than 3% of its value prior to Cr^{VI} addition. The inset in Fig. 1 shows the cathodic current spike more clearly and indicates that it occurs for both aerated and deaerated solutions, with approximately equal peak area. Table I lists the area of the current spike for several final concentrations of Cr^{VI}. Note that the spike area decreased by ~50% while Cr^{VI} decreased by three orders of magnitude. The mean spike area for 5 mM to 5 μ M [Cr^{VI}] was 1.56×10^{-3} C/cm² on the copper electrode. Figure 2 shows the current spikes for concentrations of Cr^{VI} from 5 mM to 5 μ M on an expanded time scale. Higher concentrations of Cr^{VI} result in greater spike height but narrower width, and the spike area remains constant to within a factor of 2. In fact, the peaks for the lowest Cr^{VI} additions, 0.5 and 0.05 μ M (not shown), are so drawn out that the smaller peak areas listed in Table I for these concentrations may be caused by measurement difficulty rather than a trend.

The decrease in current following the spike has two implications. First, the cathodic processes occurring on the Cu electrode before Cr^{VI} addition are greatly inhibited by Cr^{VI} or its reduction products. Second, the continuing reduction of Cr^{VI} is inhibited after the current spike, so that a steady-state reduction current for Cr^{VI} is not observed. Based on the known redox chemistry of Cr^{VI} and previous reports on electrochemical Cr^{VI} reduction,^{11–17} we tentatively attribute the cathodic spike to reduction of solution Cr^{VI} to an adsorbed film of Cr^{III} oxyhydroxide.

Figure 3 provides additional evidence for the presence of an

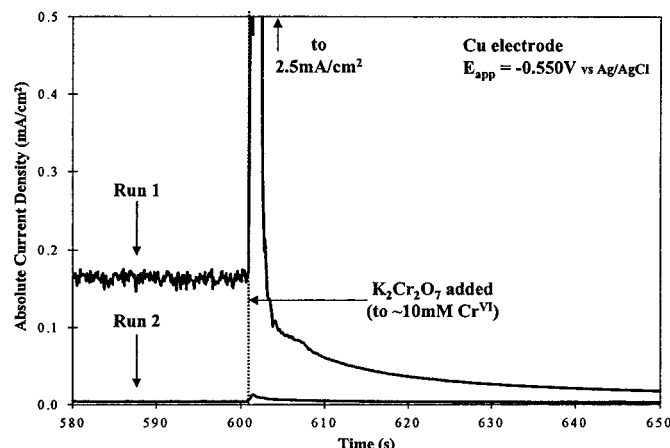


Figure 3. Effect of previous Cr^{VI} exposure on current response of copper electrode at constant potential (−0.550 V vs. Ag/AgCl) in stirred, deaerated 0.1 M NaCl. Cr^{VI} was injected (to ~10 mM) as indicated. Run 1 is a freshly polished electrode. For run 2, the electrode was rinsed and placed in fresh electrolyte.

irreversibly adsorbed species on the copper electrode. Run 1 shows the current spike and rapid inhibition upon addition of Cr^{VI} to deaerated 0.1 M NaCl as observed in Fig. 1. Following this experiment the electrode was rinsed with water, replaced in fresh deaerated electrolyte, and monitored potentiostatically to yield run 2 in Fig. 3. The current is greatly decreased compared to run 1 (<0.01 vs. ~0.17 mA/cm²) despite the absence of Cr^{VI} in solution. Upon injection of Cr^{VI}, only a minute current spike is observed (spike height <0.02 mA/cm²) compared to a freshly polished electrode (spike height ~2.5 mA/cm²). The results indicate that an adsorbed layer is formed upon the initial injection of Cr^{VI} that remains after rinsing the electrode. Since the current spike observed upon Cr^{VI} injection occurred immediately prior to the inhibition of reduction currents, the events taking place during the spike must be critical to the inhibition mechanism.

A series of constant potential experiments were conducted to examine the spike area dependence upon potential, with the results presented in Table II. The applied potential has little effect on the spike area over the range studied for Cu electrodes. The average spike area from 26 injection experiments for the potential range of −0.200 to −1.000 V was $1.2 \times 10^{-3} \pm 0.61 \times 10^{-3}$ C/cm².

The potential dependence of O₂ reduction was examined with hydrodynamic voltammetry, shown in Fig. 4 for copper, platinum, and GC electrodes. Platinum and GC electrodes offer wider potential ranges than Cu, particularly for positive potentials. Although the current densities for O₂ reduction differ for the three electrodes, the potentials observed for O₂ and Cr^{VI} reduction follow similar trends as expected from thermodynamic considerations. In aerated Cr^{VI}-free solutions, the O₂ reduction current begins to increase be-

Table I. Concentration dependence of Cr^{VI} reduction spike on Cu electrode.

	Mean					
Potential (V)	−0.600	−0.600	−0.600	−0.600	−0.600	−0.600
[Cr ^{VI}] (M) ^a	5×10^{-3}	5×10^{-4}	5×10^{-5}	5×10^{-6}	5×10^{-7}	5×10^{-8}
Spike area (C/cm ²)	2.2×10^{-3}	1.4×10^{-3}	1.6×10^{-3}	1.1×10^{-3}	5.0×10^{-4}	6.0×10^{-4}
Cr reduced (nmol/cm ²)	7.5	4.9	5.5	3.6	1.8	2.0
	1.56×10^{-3}					
	5.4 ± 1.6^b					

^a Final concentration of total Cr^{VI} after injection into deaerated 0.1 M NaCl.

^b Mean \pm standard deviation for first four columns.

Table II. Potential dependence of Cr^{VI} reduction.

Cu electrode	Potential (V vs. Ag/AgCl) ^a	-0.2 to -0.3	-0.3 to -0.5	-0.5 to -0.7	-0.7 to -0.9	-0.9 to -1.0
[Cr ^{VI}] (M)	0.005	0.005	0.005	0.005	0.005	0.005
Spike area (C/cm ²)	1.2 × 10 ⁻³	1.1 × 10 ⁻³	1.2 × 10 ⁻³	1.1 × 10 ⁻³	1.7 × 10 ⁻³	1.7 × 10 ⁻³
Cr reduced (nmol/cm ²)	4.0	3.9	4.0	3.9	6.0	6.0
Standard deviation	0.5	0.8	2.1	3.2	n/a	n/a
N	2	4	13	6	1	1
GC electrode						
Potential (V)	+0.600	+0.400	+0.350	+0.300	+0.250	+0.200
[Cr ^{VI}] (M)	0.005	0.005	0.005	0.005	0.005	0.005
Spike area ^b (C/cm ²)	5.4 × 10 ⁻⁶	8 × 10 ⁻⁸	9.5 × 10 ⁻⁵	1.3 × 10 ⁻³	2.1 × 10 ⁻³	2.2 × 10 ⁻³
Cr reduced (nmol/cm ²)	0.0	0	0.3	4.6	7.4	7.7

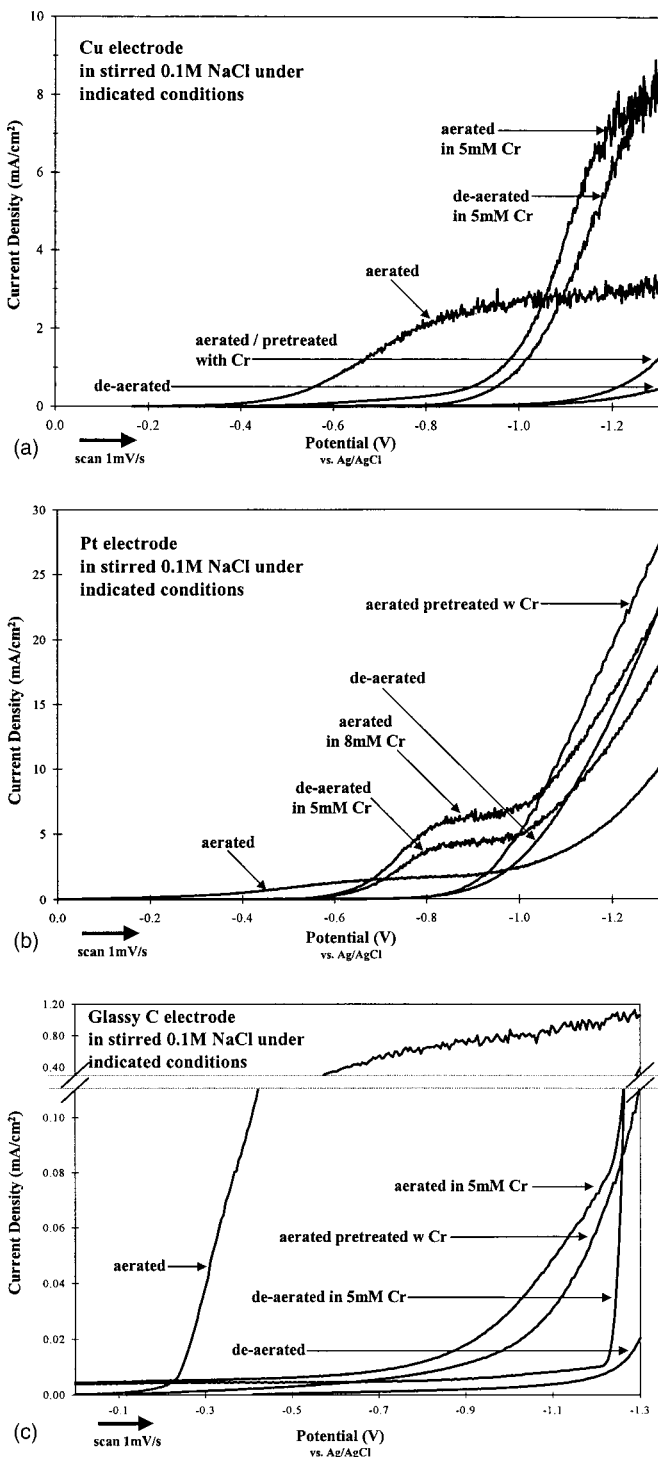
^a A range of potentials indicates that the spike area is the mean of N runs with Cr^{VI} injection at a potential in that range.^b Background charge in the absence of Cr^{VI} was subtracted.^c For 7 runs in the potential range +0.25 to -0.40 V.

Figure 4. (a) Current response vs. potential for a copper electrode in stirred 0.1 M NaCl. Conditions indicated. Potential was scanned negative from open circuit at 0.001 V/s. Pretreatment with Cr indicates that the electrode was rinsed with water after a previous scan in Cr^{VI}-containing solution, then replaced in Cr^{VI}-free electrolyte. (b) Same as a but using a platinum electrode. (c) Same as a but using a GC electrode.

tween -0.200 and -0.400 V on Cu (Fig. 4a). With constant stirring, the current increases as the potential is scanned negative, then levels off to a mass transported limited value. The same experiment in deaerated electrolyte yields little current until very negative potentials (negative of -1.2 V). The experiments were repeated (both aerated and deaerated) in the presence of 5 mM Cr^{VI} with the results

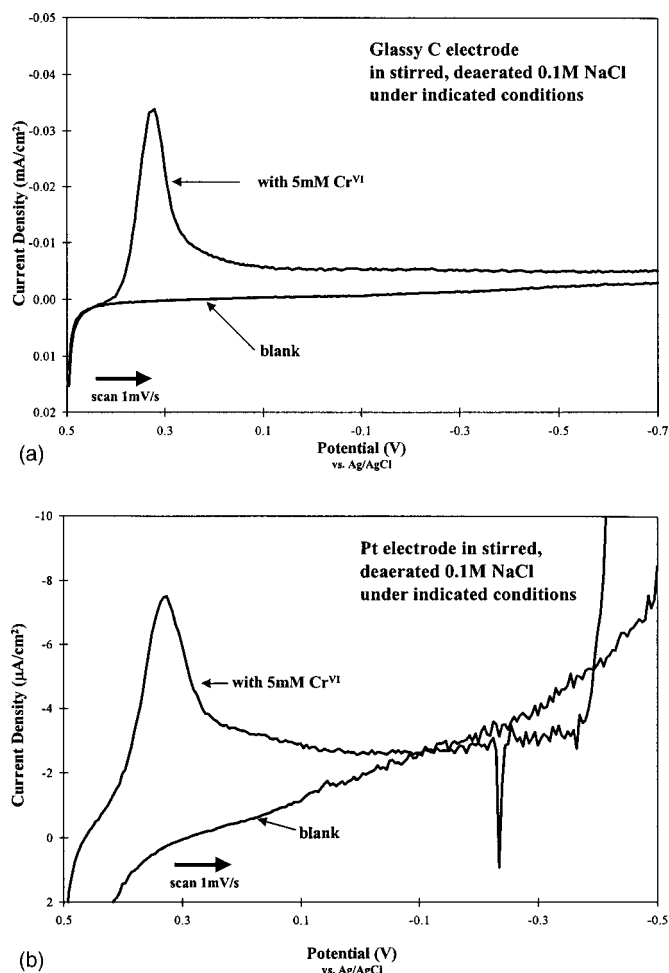


Figure 5. (a) Current response *vs.* potential for a GC electrode in stirred, deaerated 0.1 M NaCl. Potential was scanned negative from +0.500 V at 1 mV/s. Cr^{VI} was added (to \sim 5 mM) for the indicated trace while the electrode was at +0.500 V. (b) Same as for a, but with a platinum electrode.

shown in Fig. 4a. The current density remains well below the current density for the aerated Cr^{VI}-free solution until the potential reaches values near -1 V. Since the current increases here for both aerated and deaerated Cr^{VI}-containing solutions this current is attributed to reduction of Cr^{VI} to Cr^{III}. For the Pt electrode (Fig. 4b) the mass-transport limited current for Cr^{VI} reduction is observed at about -0.9 V. Finally, each electrode was removed, rinsed, and replaced in fresh Cr^{VI}-free aerated solution after a negative scan in Cr^{VI} solution. The current after this pretreatment was similar to that in the Cr^{VI}-containing solutions, showing little current attributable to oxygen reduction. Since the catalytic properties of Cu, Pt, and GC for O₂ reduction differ substantially, the products, potentials, and limiting current densities differ also. However, Cr^{VI} exposure has the same effect on all three electrodes. A reduction spike such as that shown in Fig. 1 is observed, the current for the ORR is greatly decreased, and a persistent film is formed that resists removal by rinsing.

Figure 5a shows a hydrodynamic voltammogram of Cr^{VI} solution on a GC electrode, starting at +0.5 V *vs.* Ag/AgCl in order to exploit the more positive potential limit of GC compared to Cu. Since the solution is stirred, a typical mass transport limited reduction should yield a steady-state current plateau. However, the reduction of Cr^{VI} yields a peak at about +0.32 V, quite similar to a peak observed on a Pt electrode in the same solution (Fig. 5b). The areas under these peaks in the potential range of +0.4 to +0.2 V are

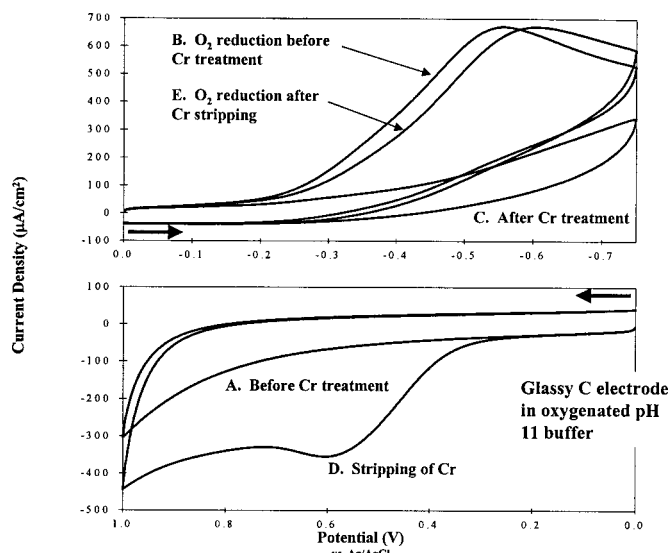


Figure 6. Cyclic voltammogram of a GC electrode in oxygenated pH 11 buffer (0.1 M BO₄³⁻/0.9 M NaCl). The scan rate was 200 mV/s. Top graph shows negative scans made before and after exposure to Cr^{VI}, as indicated. Bottom scan shows scans from 0 to +1.000 V, as indicated. Between scans B and C the electrode was pretreated with chromate as outlined in the text.

approximately 2.8×10^{-3} C/cm² for GC and 6.5×10^{-4} C/cm² for Pt.

Cyclic voltammetry was used to examine the reversibility of the adsorption process and its effect on oxygen reduction current. The results are shown in Fig. 6. Scans A and B show the current response of a GC electrode in an oxygenated pH 11 buffer solution when scanned in both positive and negative directions. A wave corresponding to the reduction of oxygen is observed on the negative scan (scan B) at about -0.600 V. The electrode was then treated with Cr^{VI} by scanning between 1.000 and -0.750 V (ending at the negative potential) in chromate ([Cr^{VI}] = 5 mM). After the GC electrode was removed, rinsed, and replaced in Cr-free electrolyte, negligible O₂ reduction current was observed on a negative scan (scan C). An anodic stripping peak was observed at about $+0.600$ V *vs.* Ag/AgCl on a subsequent positive scan (scan D), with an approximate area of 3.8×10^{-4} C/cm². After stripping, the O₂ reduction wave returned (scan E) with nearly identical current/potential response to the background scan (scan B).

The reduction peak in Fig. 5a was examined more closely using potential step experiments on GC electrodes. Figure 7 shows the results of potential steps from +0.750 V to the indicated potentials in 5 mM Cr^{VI}, with the hydrodynamic voltammogram of Fig. 5a shown for comparison. The insets show current transients when the potential is stepped, and the arrows indicate the potential to which the step was made. If the potential was stepped to a value more positive than the Cr^{VI} reduction peak of the voltammogram, no current spike was observed. When the potential was stepped to values negative of the hydrodynamic peak the current spike appears, with a shape that depends on potential. As the step becomes more negative the spike becomes narrower and the height increases. The area of the spikes shown in Fig. 7 are plotted in Fig. 8 (open squares) and listed in Table II. Despite significant variation in peak height, the area is fairly constant with potential in the range +200 to -400 mV. This limiting value corresponds to 8.1×10^{-4} C/cm² of reduction for seven potential steps in the range of +0.250 to -0.400 V.

The GC electrodes used in the potential step experiments of Fig. 7 were removed (under potential control), rinsed, and replaced in fresh aerated 0.1 M NaCl. They were then held at -1.000 V for 60 s to reduce any surface species. Following this pretreatment, the

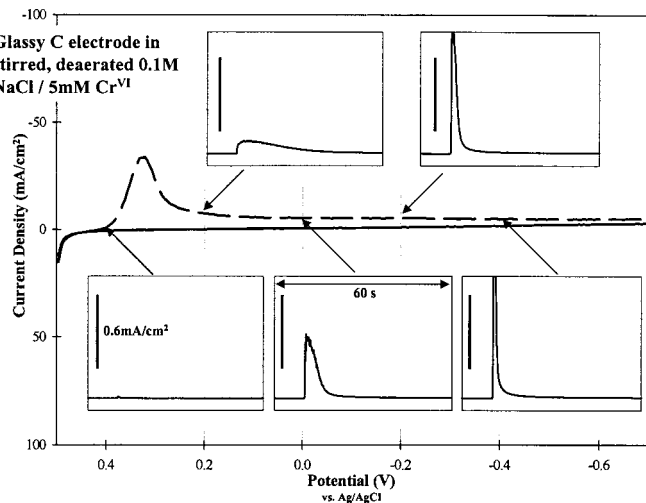


Figure 7. Potential-step experiments using GC electrodes in stirred, deaerated 0.1 M NaCl with 5 mM Cr^{VI}. The potential was held at +0.750 V and stepped to potentials indicated by the arrows. Insets show current response *vs.* time at the moment the potential was changed overlayed onto Fig. 5a. The vertical scale bar represents 0.6 mA/cm² for all insets, and each inset covers 60 s on the time axis.

potential was scanned from the OCP to -1.300 V at 5 mV/s with aeration and stirring. Figure 8 (solid circles) shows a plot of the current density at -0.600 V (from the hydrodynamic voltammetry) *vs.* the size of the potential step used to construct Fig. 7. Based on Fig. 4c, the current at -0.60 V in aerated, Cr-free electrolyte corresponds to O₂ reduction. Figure 8 shows a strong inverse correlation between the observed current spike area in Cr^{VI} solution and the O₂ reduction current following Cr^{VI} exposure. Stated differently, the Cr^{VI} reduction spike area (Fig. 8) and Cr^{VI} reduction peak (Fig. 5a) correspond directly to the onset of O₂ reduction inhibition. The results also indicate that Cr^{VI} does not adsorb strongly enough at potentials positive of the reduction peak to remain on the electrode after rinsing. If it did, the constant/potential pretreatment before hydrodynamic voltammetry should reduce the adsorbed Cr^{VI} layer to Cr^{III} and some inhibition should have been observed.

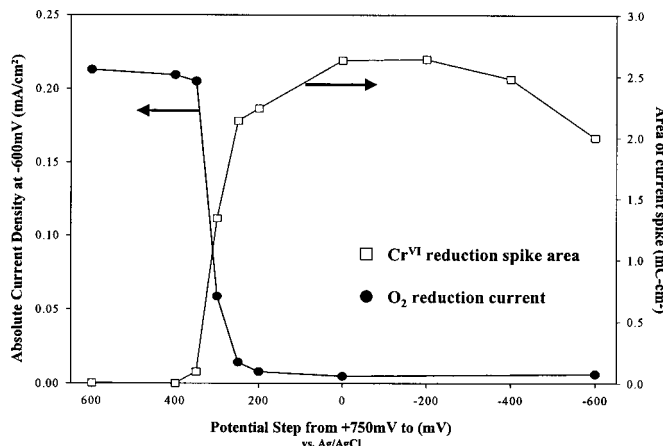


Figure 8. Correlation between onset of Cr^{VI} reduction spike and inhibition of oxygen reduction on GC electrodes. The Cr^{VI} reduction spike area () is for potential step experiments from +0.750 V to the indicated value in 5 mM Cr^{VI} (as in Fig. 7). The current density (●) value is taken at -0.600 V from a hydrodynamic voltammogram (as in Fig. 4) in aerated 0.1 M NaCl following the step to the indicated potential.

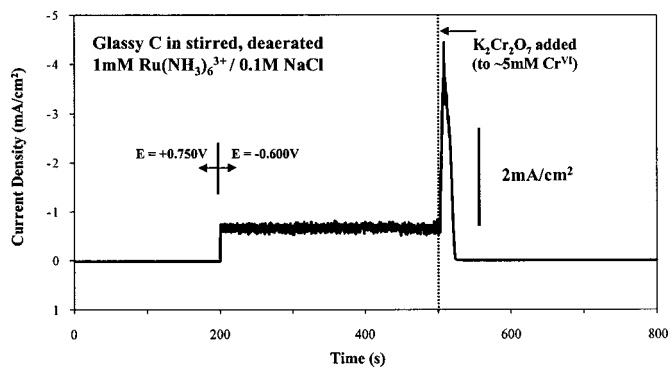


Figure 9. Current response of a GC electrode *vs.* time for stirred, deaerated 0.1 M NaCl containing 1 mM Ru(NH₃)₆³⁺. At 200 s, the potential was stepped from +0.750 to -0.600 V. At 500 s Cr^{VI} was injected (to ~5 mM).

Given the well-established electrocatalysis of O₂ reduction by chemisorption,¹⁸ it is likely that part of the mechanism of ORR inhibition by chromate is blockage of adsorption sites by a Cr^{III} layer. A Cr^{III} layer may also be an effective barrier to electron transfer, even if chemisorption is not involved. To investigate this possibility, the reduction of Ru(NH₃)₆³⁺ was studied on both copper and GC electrodes, and the oxidation of ferrocene in acetonitrile was examined on GC. Both systems are well-known examples of outer-sphere redox processes, in which adsorption to the electrode is not involved in the electron transfer.²¹⁻²³ Figure 9 shows the steady-state current for a GC electrode in a stirred solution of 1 mM Ru(NH₃)₆³⁺ (in 0.1 M NaCl) at an initial potential of +750 mV. When the potential is stepped to -600 mV at 200 s, the mass transport limited reduction of Ru(NH₃)₆³⁺ produces a current density of ~0.7 mA/cm². At *t* = 500 s, Cr^{VI} was injected to a level of 5 mM, producing a current spike similar to those shown in Fig. 1. After this spike, the Ru(NH₃)₆³⁺ reduction current decreased to 0.54% of its mass transport limited value. Ru(NH₃)₆³⁺ reduction was inhibited on a copper electrode in a similar fashion (not shown). The reduction current for a stirred solution containing 0.5 mM Ru(NH₃)₆³⁺ in the absence of Cr^{VI} was ~0.8 mA/cm² at -0.600 V on a Cu electrode. After pretreatment with 5 mM Cr^{VI} at a constant potential of -0.600 V, the electrode was removed, rinsed, and replaced in fresh 0.5 mM Ru(NH₃)₆³⁺ in the absence of Cr^{VI}. The Ru(NH₃)₆³⁺ reduction current at -0.600 V decreased to ~3% of its previous value. Figure 10 shows a cyclic voltammogram on a GC electrode in 1 mM ferrocene in acetonitrile (with 0.1 M tetrabutylammonium tetrafluoroborate background electrolyte), and for the same electrode after pretreatment with 5 mM Cr^{VI} at a constant potential of -0.600 V. The oxidation and reduction waves of ferrocene are clearly apparent for the untreated electrode but current on the treated electrode is nearly absent.

Discussion

Known chemistry of Cr^{VI} leads to the conclusion that the product of Cr^{VI} reduction at the electrode surface leads to Cr^{III}. Cr^V (as CrO₄³⁻) and Cr^{IV} have been reported in pulse radiolysis experiments, but their lifetimes are in the submillisecond region in aqueous solutions.²⁴ They rapidly disproportionate to form Cr^{VI} and Cr^{III}, but they have been characterized as transient species. Once Cr^{III} has been formed, presumably as a hydrated Cr⁺³ ion, it polymerizes to yield an insoluble Cr^{III} oxyhydroxide.^{8,25} The rate of the Cr^{III} polymerization is strongly dependent on both Cr^{III} concentration and pH, and it is not clear from the present experiments how fast the oxyhydroxide film forms after Cr^{VI} reduction. However, it is clear that the resulting film is irreversibly adsorbed on the electrode surface, and is removed only at quite positive potentials (>0.5 V *vs.* Ag/AgCl).

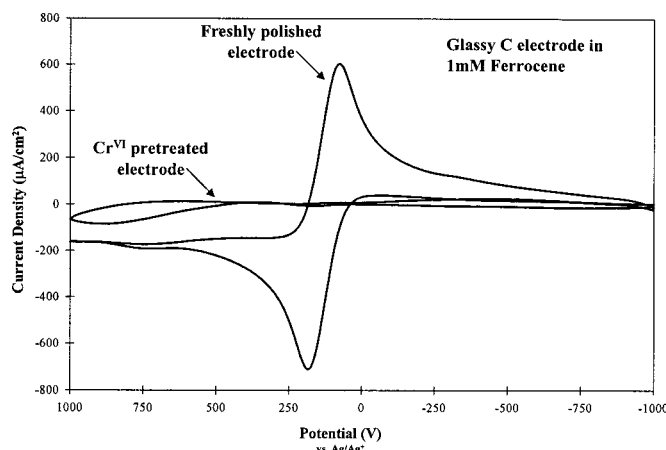


Figure 10. Cyclic voltammograms of GC electrode in quiescent, deaerated acetonitrile containing 1 mM ferrocene and 0.1 M tetrabutylammonium tetrafluoroborate. Pretreatment was performed as outlined in the text. The potential was scanned at 1000 mV/s starting at -1.000 V.

Under the assumption that the process occurring during the current spike in Fig. 1-3 is the reduction of Cr^{VI} to Cr^{III} , the area of the spike can be used to calculate the quantity of Cr^{VI} reduced via Faraday's law. The mean spike area on GC of $2.4 \times 10^{-3} \text{ C/cm}^2$ for 5 mM $[\text{Cr}^{\text{VI}}]$ (Table II) corresponds to 8.4 nmol/cm^2 of Cr^{III} . Additional Cr^{III} coverages are listed in Tables I and II. Classical experiments on Cr^{VI} reduction on Pt reported deposition of 1.9 and 2.2-3.0 nmol Cr/cm^2 .^{11-14,16} Using the octahedral geometry of Cr^{III} and assuming a bond length of $\sim 0.19 \text{ nm}$ for $\text{Cr}-\text{O}$ bonds,²⁶ a close-packed Cr^{III} monolayer is predicted to contain 2-6 nmol of Cr/cm^2 depending upon orientation of the Cr^{III} octahedron. An examination of hydroxylated Cr_2O_3 thin films in high vacuum using X-ray

photoelectron spectroscopy, total dissolved solids method, low energy electron diffraction, and scanning tunneling microscopy reported a Cr^{III} surface density of $1.9 \times 10^{15} \text{ atoms Cr/cm}^2$, or 3.2 nmol Cr/cm^2 .²⁷ The projected areas were used to calculate the Cr coverages herein, and roughness would increase the microscopic surface area and apparent coverage by a factor of about 1.5 to 2.0 compared to a flat surface. Within the uncertainty caused by surface roughness and film geometry, the present results as well as those reported by Kolthoff¹¹ for Pt electrodes indicate formation of a monolayer of Cr^{III} on Cu electrodes. The Cr^{III} coverage observed on GC was somewhat higher than that on Cu, but still corresponds to 1-2 monolayers. This coverage varied little over wide ranges of Cr^{VI} concentration and electrode potential.

Before considering the anticorrosion properties of the Cr^{III} monolayer, two aspects of its formation deserve special note. First, it forms at potentials of approximately $+0.30$ V vs. Ag/AgCl ($+0.50$ V vs. NHE) or more negative on Cu, Pt, and GC surfaces (Fig. 5,7-8). In fact, an examination of the Pourbaix diagram for chromium shows that for solutions of pH 6-7 (as for 0.1 M NaCl) the $\text{Cr}^{\text{VI}}-\text{Cr}^{\text{III}}$ reduction potential is near this value depending on the hydration state of the ions.²⁸ Consequently, the OCP of Cu (~ -0.1 V vs. Ag/AgCl) or AA2024 (~ -0.6 V vs. Ag/AgCl) is sufficiently negative to rapidly form a Cr^{III} monolayer. Under most if not all conditions expected to occur for AA2024-T3 in field applications, the potential will be sufficiently negative to reduce Cr^{VI} to Cr^{III} , and to form the Cr^{III} monolayer, even if the solution Cr^{VI} concentration is at the micromolar level. Second, the Cr^{VI} reduction is self-inhibiting, in the sense that further reduction of Cr^{VI} is extremely kinetically hindered by the Cr^{III} monolayer. Based on Fig. 4, Cr^{VI} reduction does not occur on electrodes covered by the Cr^{III}

monolayer until the potential is negative of -0.8 V vs. Ag/AgCl . Thus the Cr^{III} layer causes more than 1.0 V of kinetic overpotential, shifting the Cr^{VI} reduction from $+0.3$ to -0.8 V vs. Ag/AgCl . This large shift is presumably what stops Cr^{III} formation at one monolayer unless the electrode potential is very negative. It is important that the OCP of AA2024-T3 is sufficiently negative to form a monolayer, but not so negative that reduction continues past a monolayer. This property permits Cr^{III} monolayer formation, but prevents bulk reduction of Cr^{VI} in the CCC or primer layers.

The self-inhibition of Cr^{VI} reduction by a Cr^{III} film is apparently inconsistent with the formation of a thick (several micrometers) $\text{Cr}^{\text{III}}-\text{Cr}^{\text{VI}}$ mixed oxide film during CCC formation. For example, the Alodine 1200 process subjects AA2024-T3 to a solution containing ~ 40 mM Cr^{VI} , plus F^- ion and ferricyanide, and chromate film formation proceeds far beyond a monolayer to a thickness of 1-5 μm . However, the conditions for CCC formation are very different from those studied here, or those anticipated in the field. The high Cr^{VI} concentration and $\text{Fe}(\text{CN})_6^-$ "accelerator" generate a high Cr^{III} concentration at the alloy surface, which polymerizes to a Cr^{III} oxyhydroxide.^{4,6} F^- etching will continue to expose fresh Al and provide reducing sites for further Cr^{VI} reduction, and the low pH in Alodine 1200 will retard Cr^{III} polymerization. Furthermore, the present work dealt with Cu surfaces as models of Cu-rich phases in AA2024-T3. Raman and infrared microscopy have revealed that the CCC is significantly thinner over Cu-rich phases, compared to the Al matrix.⁷ Inhibition of $\text{Fe}(\text{CN})_6^-$ redox mediation or of Cr^{VI} reduction by a Cr^{III} film on Cu-rich phases would account for slow CCC formation on Cu, and is consistent with the present observations.

Figure 8 indicates a strong correlation between Cr^{III} film formation and O_2 reduction inhibition. It is tempting to conclude that the Cr^{III} film is acting as a "barrier" to the electrolyte, thus preventing O_2 reduction or alloy dissolution. However, a hydrated monolayer would be an imperfect barrier, and would permit electron tunneling and probably permeation by O_2 . The results permit identification of some more definite properties of the barrier film that are important to inhibition of the ORR. First, the Cr^{III} film should block sites for O_2 chemisorption, thus greatly reducing the electrocatalytic activity of the surface. Without chemisorption, slow kinetics decreases the effective O_2 reduction potential from approximately $+0.8$ V (vs. NHE) down to the outer sphere reduction potential of about -0.5 V (vs. NHE).¹⁹ At the outer sphere reduction potential, O_2 is reduced to superoxide, which disproportionates in solution to eventually form HO_2^- or H_2O_2 . With chemisorption blocked, the catalytically inactive surface significantly decreases the driving force for O_2 reduction, resulting in partial or complete ORR inhibition.

Since Cr^{VI} is itself an oxidizing agent, it may react with the same surface sites as O_2 . As shown in Fig. 4, Cr^{VI} reduction is slow in the absence of adsorption. It is quite likely that both O_2 and Cr^{VI} adsorb to similar sites on Cu, presumably bare copper atoms. The difference is that O_2 is reduced and eventually desorbed, while Cr^{VI} reduction leads to permanent occupation of the site. Since Cr^{III} is substitution inert, the Cr^{III} oxyhydroxide film is quite stable, and blocks O_2 adsorption indefinitely.

In addition to occupation of catalytic sites, a Cr^{III} monolayer can also inhibit electron transfer. Numerous reports have shown that electrons can tunnel through nonconducting monolayers, with an exponential dependence of tunneling rate on monolayer thickness. For example, electron transfer through an aliphatic hydrocarbon monolayer yields a linear plot of the log of the electron transfer rate vs. layer thickness, with a slope of -1 \AA^{-1} .²² In other words, each \AA of monolayer thickness causes a $1/e$ decrease in electron tunneling rate. A Cr^{III} oxyhydroxide made under ultrahigh vacuum conditions is $\sim 4 \text{ \AA}$ thick.²⁷ By itself, such a monolayer would decrease the electron tunneling rate by e^{-4} , or to $\sim 2\%$ of the rate without the monolayer. However, the Cr^{III} film may adsorb a layer of Cr^{VI} to

form a Cr^{III}-Cr^{VI} mixed oxide.⁸ Such a bilayer would decrease the tunneling rate by at least another factor of e⁻⁴. The strong inhibition of electron transfer to Ru(NH₃)₆⁺³ and from ferrocene apparent in Fig. 9 and 10 is consistent with decreased tunneling rates to outer sphere redox systems (presumably including O₂/O₂⁻), but the present results permit only a semiquantitative estimate of the magnitude of the effect.

The present conclusions add significantly to the emerging understanding of the origin of the unparalleled performance of chromate-based anticorrosion coatings. Past reports identified the storage and release of Cr^{VI} in conversion coatings and chromated primers as essential prerequisites for the "self healing" observed in chromate coatings. The release and migration of active Cr^{VI} species from a chromate coating to a newly formed defect appears to be essential for the long effective lifetimes of chromate coatings. The present results address the fate of Cr^{VI} once it migrates to a corroding defect. It is clear that reduction of Cr^{VI} leads to a stable, insoluble Cr^{III} film, which apparently does not grow beyond a monolayer in dilute, neutral aqueous solutions. The Cr^{VI} is a "site-directed" inhibitor in that it is adsorbed to an active site, then is reduced to permanently block the site. We stress ORR inhibition as a principal target of chromate inhibition, but certainly not exclusively so. The irreversible reduction Cr^{VI} to form a Cr^{III} monolayer could also afford protection to anodic sites, such as Mg rich s-phase intermetallic particles. More generally, there remain several possible actions of Cr^{VI} as a corrosion inhibitor which were not considered here, but the results indicate that O₂ reduction is certainly inhibited by Cr^{VI}, and provide important detail about the inhibition mechanism. The unusual combination of storage, release, reduction, and inhibition by Cr^{VI} inhibitors make them outstanding agents for corrosion protection. During the search for environmentally benign alternatives, these properties should be duplicated as much as possible.

Conclusions

1. Cr^{VI} inhibits reduction of oxygen under conditions relevant to corrosion.
2. The mechanism of inhibition involves a reduction and irreversible adsorption of Cr^{III} to the surface of the electrode to block sites of adsorption. Once adsorption sites are blocked, O₂ chemisorption is prevented and O₂ becomes a much weaker oxidizing agent.
3. The Cr^{III} film is formed in near-monolayer quantities.
4. The Cr^{III} film is nonconductive and inhibits outer-sphere redox processes.
5. The Cr^{III} film formed inhibits further Cr^{VI} reduction until very negative potentials can drive outer sphere electron transfer.

6. The reduction of Cr^{VI} and inhibition of O₂ reduction occur over the entire potential range relevant to corrosion of AA2024-T3 alloys.

Acknowledgments

This work was supported by the Air Force Office of Scientific Research as part of the Ohio State "MURI." The authors appreciated useful scientific discussions with Gerald Frankel, Martin Kendig, and R. G. Buchheit. The authors also thank Takashi Itoh for his assistance in translation of Japanese journal articles.

The Ohio State University assisted in meeting the publication costs of this article.

References

1. G. O. Ilevbare and J. R. Scully, *J. Electrochem. Soc.*, **148**, B196 (2001).
2. M. Kendig and S. Jeanjaquet, *Surf. Coat. Technol.*, **140**, (2001).
3. W. J. Clark, J. D. Ramsey, R. L. McCreery, and G. S. Frankel, *J. Electrochem. Soc.*, **149**, B179 (2002).
4. L. Xia and R. L. McCreery, *J. Electrochem. Soc.*, **146**, 3696 (1999).
5. M. W. Kendig, A. J. Davenport, and H. S. Isaacs, *Corros. Sci.*, **34**, 41 (1993).
6. L. Xia and R. L. McCreery, *J. Electrochem. Soc.*, **145**, 3083 (1998).
7. W. R. McGovern, P. Schmutz, R. G. Buchheit, and R. L. McCreery, *J. Electrochem. Soc.*, **147**, 4494 (2000).
8. L. Xia, E. Akiyama, G. Frankel, and R. L. McCreery, *J. Electrochem. Soc.*, **147**, 2556 (2000).
9. J. Zhao, G. Frankel, and R. L. McCreery, *J. Electrochem. Soc.*, **145**, 2258 (1998).
10. V. Guillaumin, P. Schmutz, and G. Frankel, *J. Electrochem. Soc.*, **148**, B163 (2001).
11. I. M. Kolthoff and A. M. S. e. Din, *J. Phys. Chem.*, **60**, 1564 (1956).
12. G. Lindbergh and D. Simonsson, *Electrochim. Acta*, **36**, 1985 (1991).
13. G. Lindbergh and D. Simonsson, *J. Electrochem. Soc.*, **137**, 3094 (1990).
14. I. Taniguchi and T. Sekine, *Denki Kagaku oyobi Kogyo Butsuri Kagaku*, **43**, 201 (1975).
15. I. Taniguchi and T. Sekine, *Denki Kagaku oyobi Kogyo Butsuri Kagaku*, **43**, 632 (1975).
16. I. Taniguchi and T. Sekine, *Denki Kagaku oyobi Kogyo Butsuri Kagaku*, **43**, 709 (1975).
17. A. F. Diaz and D. Schermer, *J. Electrochem. Soc.*, **132**, 2571 (1985).
18. R. Adzic, in *Electrocatalysis*, J. Lipkowski and P. Ross, Editors, p. 197, Wiley-VCH, New York (1998).
19. H.-H. Yang and R. L. McCreery, *J. Electrochem. Soc.*, **147**, 3420 (2000).
20. D. A. Jones, *Principles and Prevention of Corrosion*, Prentice Hall, Upper Saddle River, NJ (1996).
21. H.-H. Yang and R. L. McCreery, *Anal. Chem.*, **71**, 4081 (1999).
22. H. O. Finklea and D. D. Hanshen, *J. Am. Chem. Soc.*, **114**, 3173 (1992).
23. H. O. Finklea, in *Electroanalytical Chemistry*, Vol. 19, A. J. Bard, Editor, p. 109, Marcel, Dekker, New York (1996).
24. G. V. Buxton and F. Djouider, *J. Chem. Soc., Faraday Trans.*, **92**, 4173 (1996).
25. H. Stunzi and W. Marty, *Inorg. Chem.*, **28**, 66 (1989).
26. K. H. Theopolis, *Encyclopedia of Inorganic Chemistry*, Wiley, New York (1994).
27. B. Maurice, S. Cadot, and P. Marcus, *Surf. Sci.*, **471**, 43 (2001).
28. M. Pourbaix, *Atlas of Electrochemical Equilibria in Aqueous Solutions*, NACE, Houston, TX (1974).